$^{12}C(p,n)^{12}N$ reaction at 135 MeV

B. D. Anderson,[1] L. A. C. Garcia,[1,*] D. J. Millener,[2] D. M. Manley,[1] A. R. Baldwin,[1] A. Fazely,[1,*] R. Madey,[1,4] N. Tamimi,[1,†] J. W. Watson,[1] and C. C. Foster[3]

[1]*Department of Physics and Center for Nuclear Research, Kent State University, Kent, Ohio 44242*

[2]*Brookhaven National Laboratory, Upton, New York 11973*

[3]*Indiana University Cyclotron Facility, Bloomington, Indiana 47405*

[4]*Hampton University, Hampton, Virginia 23668*

(Received 29 December 1995)

We report observations from the (p,n) reaction on ^{12}C at 135 MeV. The experiment was performed with the beam-swinger neutron time-of-flight system at the Indiana University Cyclotron Facility. Neutrons were detected in large-volume plastic scintillation detectors located in three detector stations at 0°, 24°, and 45° with respect to the undeflected beam line; the flight paths were 91 m, 91 m, and 74 m, respectively. Overall time resolutions of about 825 ps provided energy resolutions of about 350 keV in the first two stations and about 425 keV in the third station. The angular distributions for states with excitation energies up to 10 MeV are presented and comparisons are made with DWIA calculations that use one-body density matrices from $0\hbar\omega$ and $1\hbar\omega$ shell-model calculations. New information is deduced on the excitation energies, widths, and spin-parity assignments for several energy levels of ^{12}N. [S0556-2813(96)02907-X]

PACS number(s): 25.40.Kv, 21.10.Hw, 21.60.Cs, 27.20.+n

I. INTRODUCTION

Nucleon-induced charge-exchange reactions provide an extremely useful probe of isovector excitations in nuclei [1]. In part, this is because cross sections and spin observables for strong transitions at medium energies are described well by distorted-wave impulse approximation (DWIA) calculations. More precisely, single-step charge exchange appears to be the dominant reaction mechanism above 100 MeV incident energy, with both t-matrix and G-matrix interactions successfully describing experimental cross sections when the one-body transition densities are known [2]. Experimentally, the energy resolution is best at low energies and we have performed a number of studies using the (p,n) reaction at 135 MeV incident energy [3–8]. These include studies of Gamow-Teller strength [4,7], stretched states [8,9], and simple particle-hole excitations in closed-shell nuclei [3,5,6].

In closed-shell nuclei, the predominantly single-step reaction excites mainly one-particle–one-hole (1p1h) final states. Such excitations are relatively easy to describe theoretically [10,11] and comparisons with experimental results can provide important tests of nuclear structure models. For example, the strongest excitations observed in the (p,n) reaction on the closed-shell nuclei ^{16}O and ^{40}Ca [5,6] are consistent with the predictions of simple shell-model calculations [12] in the Tamm-Dancoff approximation (TDA), which assumes that the target is a closed core and that the final states are made up of only 1p1h configurations. Although these shell-model calculations are able to reproduce the relative strengths and the excitation energies fairly well, the absolute strengths calculated in the DWIA are generally too large by a factor of 2 or more. To obtain an understanding of the absolute strengths, the inclusion of 2p2h correlations in the initial and final states is required. This is done in the extension of the TDA to the random-phase approximation (RPA). The quenching, or enhancement, of strength for collective states can be clearly demonstrated in simple but realistic schematic models [10,11].

The RPA correlations, and others, can be included in more sophisticated shell-model calculations, which avoid the violations of the Pauli principle inherent in the RPA. For example, in the calculations and analyses of Gareev *et al.* [13] for ^{16}O, which include selected configurations up to $3\hbar\omega$, the normalization factors required for the DWIA calculations are much closer to unity. More recently, calculations have been performed for ^{16}O, which include all configurations up to $4\hbar\omega$ [14,15]. In Ref. [15], a factor of 2 quenching with respect to the TDA was found for the spin-dipole matrix element between the ^{16}O and ^{16}N ground states. The basis sizes for such shell-model calculations are typically very large unless a realistic symmetry scheme can be used to truncate the bases; furthermore, consistency problems not present for $0\hbar\omega$ or $1\hbar\omega$ calculations should be addressed [15,16].

The situation is very similar for open-shell nuclei, as exemplified by our studies of the self-conjugate nuclei ^{20}Ne, ^{24}Mg, ^{28}Si, and ^{32}S [7,8]. Most of the experimental (p,n) spectra and angular distributions are described reasonably well by large-basis shell-model calculations (still at the $0\hbar\omega$ or $1\hbar\omega$ level), although some specific transitions are described poorly. As for the closed-shell nuclei, the theoretical cross sections typically need to be renormalized by 10% to greater than 50% to agree in magnitude with experiment. In these cases, the multi-$\hbar\omega$ bases are so large that extended-basis shell-model calculations have not been performed.

The $^{12}C(p,n)^{12}N$ reaction that we study in this work pro-

*Present address: Physics Department, Southern University, Baton Rouge, LA 70813.

†Present address: Oncology Service Corporation, Maryland General Cancer Center, 821 N. Eutaw, Baltimore, MD 21201.

vides a more realistic example for tests of extended-basis shell-model calculations. Although such calculations have not yet been performed, the basis sizes are comparable to those for $A=16$ and the calculations should be possible. There have been many studies of charge-exchange reactions on ^{12}C and references to the older literature may be found in recent papers devoted to (n,p) [17,18] and (p,n) [19] studies. The most prominent peaks in charge-exchange spectra are due to the 1^+ ground state, a 2^- spin-dipole state at $\sim$4 MeV, and 1^- dipole and spin-dipole strength centered around 7 MeV. The resolution in this work is sufficient to exhibit clearly two more peaks and to extract cross sections for a number of other states by peak fitting.

The experimental procedure is given in Sec. II. The data reduction is described and spectra are presented in Sec. III. The structure and reaction calculations are described in Sec. IV, where existing information on the positive-parity and negative-parity states is summarized and interpreted in terms of shell-model calculations with the Cohen-Kurath [20] and Millener-Kurath [21] interactions, respectively. Since most of the ^{12}N states of interest are unbound and possess substantial proton decay widths, calculated Coulomb energy shifts and decay widths are used to relate the states of ^{12}N to those of ^{12}B, which are better known. A detailed comparison between the measured angular distributions and theory is made in Sec. V; the results are summarized, and conclusions drawn, in Sec. VI.

II. EXPERIMENTAL PROCEDURE

The measurements were performed at the Indiana University Cyclotron Facility with the beam-swinger system. The experimental arrangement and data reduction procedures were similar to those described previously [3,4]. Neutron kinetic energies were measured by the time-of-flight (TOF) technique. A beam of 135-MeV protons was obtained from the cyclotron in narrow beam bursts typically 350 ps long, separated by 133 ns. Neutrons were detected in three detector stations at 0°, 24°, and 45° with respect to the undeflected proton beam. The flight paths were 90.9 m, 90.8 m, and 74.4 m ($\pm$0.2 m), respectively. The neutron detectors were rectangular bars of fast plastic scintillator 10.2 cm thick. Two separate detectors, each 1.02 m long by 0.25 m high, were combined for a total frontal area of 0.51 m^2 in the 0° station, and two detectors, each 1.02 m long by 0.51 m high, were combined for a total frontal area of 1.04 m^2 in the 24° station. The 45° station had two detectors, one 1.02 m long by 0.51 m high and the second 1.02 m long by 1.02 m high, for a total frontal area of 1.55 m^2. Each neutron detector had tapered Plexiglass light pipes attached on the two ends of the scintillator bar, coupled to 12.8-cm diameter phototubes. Timing signals were derived from each end and combined in a mean-timer circuit [22] to provide the timing signal from each detector. Overall time resolutions of about 825 ps were obtained, including contributions from the beam burst width (350 ps) and energy spread (480 ps), energy loss in the target (300 ps), neutron transit times across the 10.2 cm thickness of the detectors (550 ps), and the intrinsic time dispersion of each detector (300 ps). This overall time resolution provided an energy resolution of about 350 keV in the first two detector stations and about 480 keV in the widest-angle station.

TABLE I. Energy levels of ^{12}N.

This work			Ref. [30]		
E_x (MeV)	J^π	Width (keV)	E_x (MeV)	J^π	Width (keV)
0.0	1^+	0	0.0	1^+	0
1.0	$2^+,2^-$		0.960	2^+	$\leqslant$20
			1.191	2^-	118
1.8	1^-		1.80	1^-	750
			2.439	0^+	68
3.2	(3^-)		3.132	2^+, 3^-	220
3.5	$(1^-,2^+)$		3.558	$(1)^+$	220
4.18(5)	2^-	836(25)	4.140	2^-+4^-	825
4.41(5)	4^-	744(25)			
5.40(5)	3^+, 3^-	385(55)	5.348	3^-	180
6.4	1^-		6.40	(1^-)	1200
7.3	1^-		7.40	(1^-)	1200

The large-volume detectors were described in more detail previously [23]. Protons from the target were rejected by anticoincidence detectors in front of each neutron detector array. Cosmic rays were vetoed by anticoincidence detectors on top as well as the ones at the front of each array.

The ^{12}C target was a 31.4 mg/cm^2 natural target (98.9% ^{12}C). The TOF spectra were obtained at 12 angles between 0° and 63°. Spectra from each detector were recorded at many pulse-height thresholds from 25 to 90 MeV equivalent-electron energy (MeVee). Calibration of the pulse-height response of each of the detectors was performed with a ^{228}Th source (which emits a 2.61-MeV gamma ray) and a calibrated fast amplifier. The values of the cross sections extracted for different thresholds were found to be the same within statistics. The values of the cross sections reported are at a threshold setting of 40 MeVee.

III. DATA REDUCTION

The experimental procedure and data reduction are similar to those described in more detail in Refs. [3,4]. Excitation-energy spectra were obtained from the measured TOF spectra using the known flight paths and a calibration of the time-to-amplitude converter. Known states in the residual nucleus ^{12}N provided absolute reference points. Excitation energies are estimated to be accurate to 0.1 MeV or better; for example, to 50 keV for several of the peaks listed in Table I. The excitation-energy spectra for five angles at roughly 12° intervals are presented in Fig. 1.

Yields for individual transitions were obtained by fitting peaks in the TOF spectra. The spectra were fitted with an improved version of the peak-fitting code of Bevington [24]. Because the proton threshold in the residual nucleus, ^{12}N, is at 0.60 MeV, all the final states are unbound except for the g.s.; consequently, we fit the (p,n) spectra using Lorentzian line shapes folded together with a Gaussian line shape to account for the experimental resolution. The Gaussian width was determined from the fit to the g.s. peak in each spectrum. We set the widths of the Lorentzians to be the widths accepted in the compilation of Ajzenberg-Selove [30], except for the strong, broad 2^-, 4^- complex at 4.3 MeV and the 3^+, 3^- peak at 5.4 MeV, which were fitted here to obtain

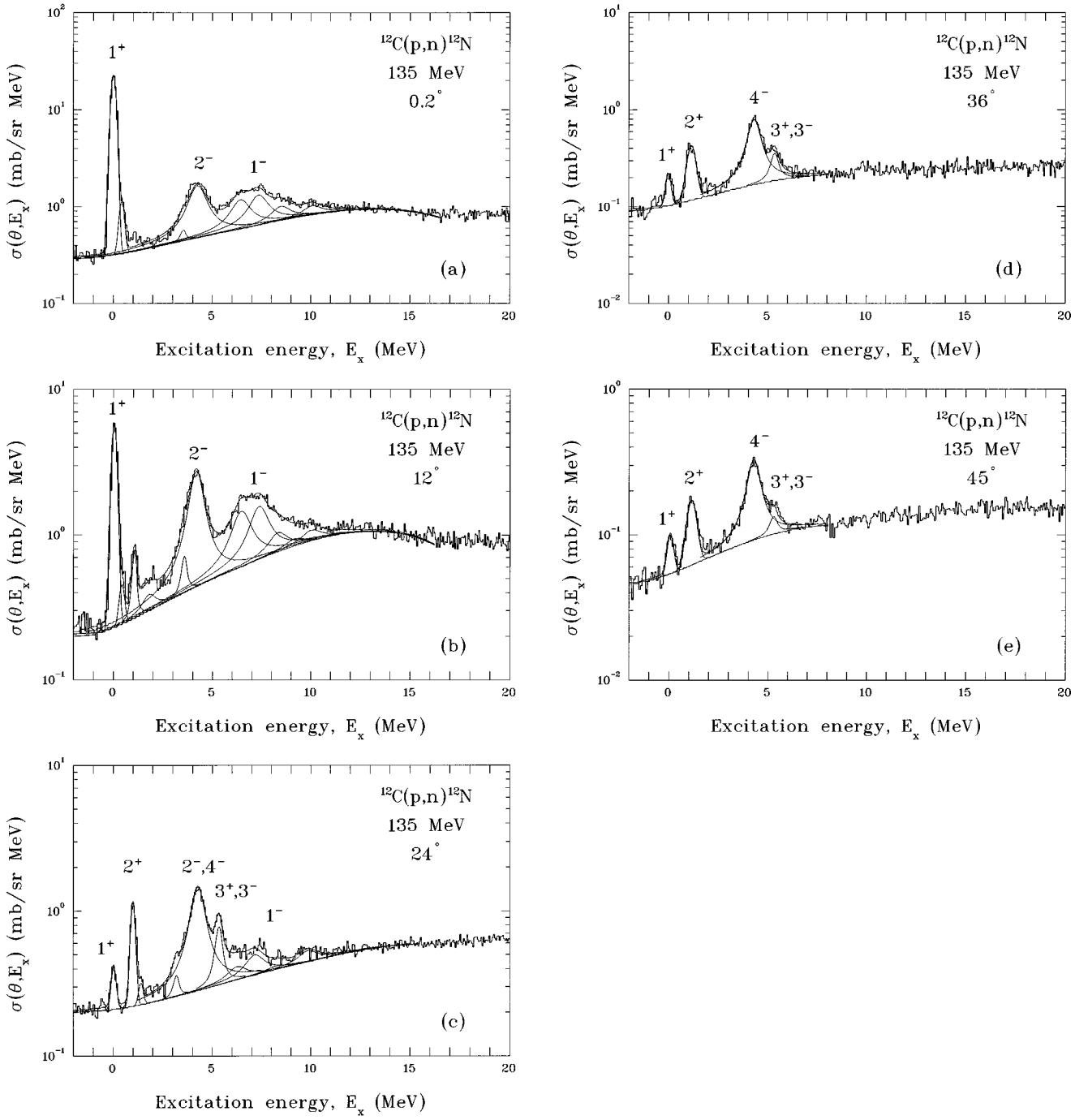

FIG. 1. Excitation-energy spectra at 0°, 12°, 24°, 36°, and 45° for the ^{12}C(p,n)^{12}N reaction at 135 MeV. Fits to the neutron time-of-flight spectra are shown. See text for discussion.

new values, as discussed below. The fits included a cubic polynomial background that provided a shape very much like that of calculated quasifree scattering [i.e., (p,pn)] spectra as presented previously [25,26]. Examples of the fitting are shown in Fig. 1. Note that a small ''tail'' is observed on the large g.s. peak, which is fitted with an additional Gaussian (see the two forward-angle spectra in Fig. 1). Such tails are commonly observed in neutron TOF spectra and arise from time slewing of lower pulse-height events. The area of this tail is ~3% of the total peak area and is included in the area for the peak. Such tails cannot be observed on the broader unbound states. In general, the fits were judged to be good. There always remains the question of the background under peaks in the continuum region. This uncertainty affects primarily the high-lying states above 6 MeV. The results we present here represent a lower limit for these levels because we are not considering contributions from the underlying continuum, such as one might obtain in a ''multipole analysis'' of the entire spectrum, for example.

We allowed the excitation energy and the Lorentzian width for the 2^-, 4^- complex to vary because we observed that both changed in a systematic way from forward angles to backward angles as the dominant level changed from the 2^- to the 4^- state. These levels are broad (~800 keV) and

excited strongly so that we could determine, with the experimental resolution of 350 keV in this work, the energies and the widths for both levels; in addition, we could extract an excitation energy and width for the 5.4-MeV peak from the two spectra, at 24° and 30°, in which the peak is most prominent. The excitation energies and the widths of states observed in this work are compared with the compilation values in Table I.

Cross sections were obtained by combining the yields with the measured geometrical parameters, the beam integration, and the target thickness. Neutron efficiencies were obtained from a Monte Carlo computer code [27], which was tested extensively at these energies [28,29]. The uncertainty in the cross section is dominated by the uncertainty in the detector efficiencies, which is estimated to be 12%. Uncertainties shown in the angular distributions are the fitting and statistical uncertainties only.

Excitation-energy spectra for the $^{12}C(p,n)^{12}N$ reaction at 135 MeV at 0°, 12°, 24°, 36°, and 45° are shown in Fig. 1. The strongest transitions are labeled by the J^π of the residual state in ^{12}N. For some of the states, the J^π assignments are known from earlier work; for the other cases, the identifications were made here by comparing the extracted angular distributions with DWIA calculations and with known analog states in ^{12}C and ^{12}B, as described below. The J^π assignments for states up to about 6 MeV in excitation energy are known quite well in the analog $T=1$ nucleus, ^{12}B, and are listed in the compilation [30]. The analogs of most of these states in ^{12}C are known also and are listed in the compilation.

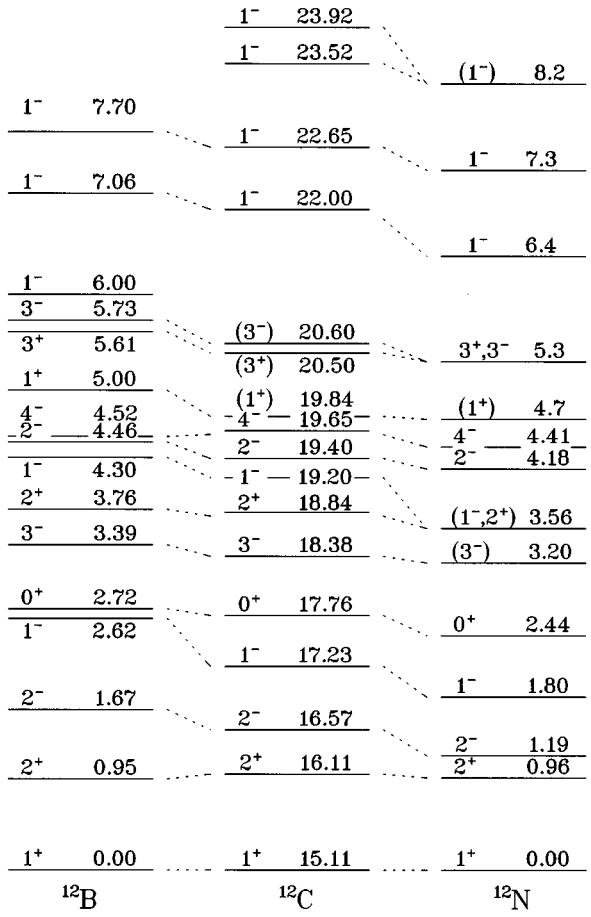

FIG. 2. Comparison of the $T=1$ energy levels in ^{12}B, ^{12}C, and ^{12}N (from this work and Ref. [30]). Energies in ^{12}C have been shifted by 15.11 MeV (the excitation energy of the analog of the ^{12}N and the ^{12}B ground states).

IV. STRUCTURE AND REACTION CALCULATIONS

In ^{12}N, the proton threshold is at 0.601 MeV and thus all levels except the ground state are particle unstable. The states of interest for our experiment, including the broad peak centered around 7 MeV, lie below the α threshold at 8 MeV. The proton decay widths of these states are generally quite large and are, in themselves, a useful test of nuclear structure models. The tabulated widths [30] come mostly from a high-resolution $^{12}C(^3He,t)^{12}N$ experiment [31], which should populate the same states as the $^{12}C(p,n)^{12}N$ reaction. In ^{12}B, the neutron-decay threshold is at 3.37 MeV and the spectrum is quite well known below 6 MeV in excitation energy. The analog states in ^{12}C are known also but a detailed interpretation of the spectrum and decay widths is made less certain on account of the possibility of isospin mixing with $T=0$ states; isospin mixing is known to exist in several instances and is generally expected to be present because states of the same space-spin structure but different isospin occur in close proximity due to an underlying supermultiplet and/or weak-coupling structure. A comparison of the $T=1$ analog states in ^{12}B, ^{12}C, and ^{12}N is presented in Fig. 2. As can be seen, the J^π assignments for the low-lying states in ^{12}N are known for only about half as many states as are known for the analogs in ^{12}B and ^{12}C. Unless otherwise indicated, if we state that a certain excitation energy and/or J^π assignment is ''known,'' we will mean that it is listed as such in the compilation of Ref. [30].

The essential features of the structure of the states in Fig. 2 can be understood from $0\hbar\omega$ and $1\hbar\omega$ shell-model calculations for the positive-parity and negative-parity states, respectively. Such calculations have been described and the one-body density-matrix elements (OBDME) required for reaction calculations tabulated in connection with previous analyses of inelastic scattering and charge-exchange experiments on ^{12}C [17,32]. In the following subsections, we give brief discussions of the spin-parity assignments, first for the positive-parity states and then for the negative-parity states. Next, we make estimates of the Coulomb-energy differences between negative-parity states of ^{12}B and ^{12}N to predict the excitation energies of states in ^{12}N from the known states in ^{12}B. The prediction of particle-decay widths for unbound states is a by-product of the same calculation. Finally, we specify the ingredients of distorted-wave calculations to compute cross sections using the nuclear structure input.

A. Positive-parity states

There are six positive-parity states below 6 MeV in ^{12}B with $J_n^\pi = 1_1^+$, 2_1^+, 0_1^+, 2_2^+, 1_2^+, and 3_1^+. The largely p-shell character of these states is evident in pickup reactions. The first five states are observed in the $^{13}C(d,^3He)^{12}B$ reaction [34] and the 3^+ state is clearly seen in the $^{14}C(p,^3He)^{12}B$ reaction [33]. The ^{12}C analogs of all six states are excited strongly in the $^{15}N(p,\alpha)^{12}C$ reaction

TABLE II. One-body density-matrix elements in LS coupling for the even-parity transitions. For each state, the first line refers to the MP4 interaction and the second to the Cohen and Kurath POT interaction.

J_n^π	E_x (MeV)[a]	$L=0,S=1$	$L=1,S=0$	$L=1,S=1$	$L=2,S=0$	$L=2,S=1$
1_1^+	−0.53	0.2886	−0.0973	0.7659		0.1681
	0.03	0.2262	−0.0327	0.7280		0.1361
2_1^+	0.91			0.3734	−0.4229	0.4008
	1.64			0.3712	−0.4479	0.5137
0_1^+	2.54			0.5578		
	4.54			0.6243		
2_2^+	3.90			0.3598	0.1316	−0.0954
	4.99			0.3899	0.1763	−0.1422
1_2^+	4.51	0.0138	−0.3117	0.0646		−0.2390
	4.45	0.0240	−0.4062	0.1135		−0.2427
3_1^+	5.04					0.2628
	4.56					0.2978

[a]Theoretical energies relative to the ground state.

[35] in accordance with p-shell predictions [36,37]. In the Cohen and Kurath models [20], only the two lowest states were included in fits to energy-level data, and the other four states cluster between 4.2 and 5.2 MeV in excitation energy for all three fitted p-shell effective interactions. With the larger data base on p-shell levels now available, similar fits reproduce the energies of all six levels quite well [38]; however, changes in the wave functions, and hence the OBDME for inelastic scattering, are small (e.g., the 0^+ state has to have essentially pure [431] spatial symmetry with $L=1$ and $S=1$). This is evident from Table II, which gives the LS-coupling OBDME for the CKPOT and MP4 [39] interactions. The LS-coupling OBDME can be scaled to obtain a fit to (e,e') form factors, as was done for the lowest 1^+ and 2^+ states by Brady *et al.* [17], and then converted to jj coupling and relative coordinates [17] for use with the distorted-wave code DW81 [40].

Higher $0\hbar\omega$ states are predicted to be excited weakly and to fall in a region where dipole and spin-dipole excitations are dominant. The lowest $2\hbar\omega$ states, which should be excited weakly, are also expected in this region. A rough estimate for the energy of the lowest $p^6(sd)^2\ 1^+$, $T=1$ state is obtained by subtracting the 6.5-MeV energy difference between the lowest 0^+, $T=2$ and 1^+, $T=1$ states in ^{16}O from the energy of the lowest $T=2$ state for $A=12$ (12.75 MeV for ^{12}B), which is thought to have a large $2\hbar\omega$ component.

B. Negative-parity states

For the negative-parity states, we use wave functions computed in the full $1\hbar\omega$ space with the Millener-Kurath (MK) interaction [21]. The general features of this calculation have been discussed by Hicks *et al.* [32] in connection with an analysis of magnetic-multipole excitations in ^{12}C seen by inelastic electron scattering. In particular, the supermultiplet symmetry and weak-coupling structure, especially for the $T=1$ states of interest here, was investigated. An extensive discussion of the distribution of dipole and spin-dipole strength for these wave functions has been given by Brady *et al.* [17] in connection with a study of the ^{12}C$(n,p)^{12}$B reaction at energies around 60 MeV. The distribution of dipole and spin-dipole strength for the fitted p-sd interactions of Warburton and Brown [38] is very similar [18] to that for the MK interaction. The OBDME necessary for the reaction calculations described in this paper are listed in Refs. [17,32].

Because the pickup strength for the removal of p-shell nucleons from ^{12}C is exhausted by the lowest two $3/2^-$ states (at 0 and ∼5 MeV) and the lowest $1/2^-$ state (at ∼2 MeV) of the core, a substantial parentage to one or more of these states is a prerequisite for the strong inelastic excitation of $A=12$ excited states. The $1\hbar\omega$ model predicts eight states below 6 MeV in ^{12}B or ^{12}N, all of which have dominant weak-coupling parentages to the $3/2^-$ ground state or the $1/2^-$ first-excited state. Experimental counterparts for seven of these states are known in ^{12}B. Only a 0^- level, a member of a $1/2_1^- \otimes 1s_{1/2}$ doublet with the 1_2^- level (at 4.30 MeV in ^{12}B), has not been identified. The MK interaction, which successfully reproduces the ordering of known $0^-,1^-$ doublets in this mass region, puts the 0^- level 0.53 MeV below the 1^- level. This assignment would put the 0^- state close to the 3.76-MeV 2^+ level in ^{12}B. A 0^- state, of unknown (and probably mixed) isospin, has been found at 18.40 MeV in ^{12}C [41], 0.8 MeV below the analog 1^- level.

A deficiency in the energy predictions from the MK interaction is that the separation between states with dominant $1s_{1/2}$ and $0d_{5/2}$ parentages is about 1 MeV too small, a feature not much improved in the fits by Warburton and Brown (see Table IV of Ref. [38]). Nevertheless, the admixtures between the $s_{1/2}$ and $d_{5/2}$ configurations seem to be correct in the sense that the very different shapes of the (e,e') form factors for the two 2^- levels are reproduced [32]. The $1s$, $0d$ admixtures are tested also by the Coulomb energy and decay-width calculations discussed in the following subsection.

Above 6 MeV, dipole and spin-dipole excitations are expected to dominate the ^{12}C$(p,n)^{12}$N cross section. These states also have dominant parentages, mostly d wave, to the low-lying core states, including now the $5/2_1^-$ and $3/2_2^-$ levels. As can be seen from Fig. 1, the only discernable peak occurs at about 7 MeV excitation energy for angles near the peak of the dipole angular distribution.

TABLE III. Coulomb energy differences between ^{12}B and ^{12}N for negative-parity states. For each weak-coupling configuration indicated in the first column, parentages for the eight states listed in the first row are given. Single-particle Coulomb energies (in MeV), calculated using the neutron energy for the specified component, are given in the next row. The parentage not accounted for by the lowest four core states is denoted by $E_>$ and is included with the $3/2_2^- \otimes d$ strength in the calculation. $\Delta E_C^{\rm th}$ is the sum of single-particle Coulomb energies $\Delta E_C^{\rm sp}$ weighted by parentages. ΔE_x is a similarly computed correction to account for the fact that the excitation energies of ^{11}C states are lower than in ^{11}B. $\Delta E_C^{\rm sp}$ and ΔE_x are used to obtain theoretical excitation energies for states in ^{12}N, which are then compared with the experimental values, ΔE being the difference in keV.

	2_1^-	1_1^-	3_1^-	0_1^-	1_2^-	2_2^-	4_1^-	3_2^-
$E_x^{\rm expt}(^{12}{\rm B})$	1.674	2.621	3.389	(3.77)[a]	4.301	4.460	4.518	5.726
$\frac{3}{2}_1^- \otimes s$	0.697	0.762			0.024	0.163		
$\Delta E_C^{\rm sp}$	2.105	1.687			[b]	[b]		
$\frac{3}{2}_1^- \otimes d$	0.195	0.074	0.879	0.002	0.002	0.476	0.815	0.034
$\Delta E_C^{\rm sp}$	2.707	2.598	2.509	2.478	2.452	2.447	2.445	2.426
$\frac{1}{2}_1^- \otimes s$		0.032		0.879	0.772			
$\Delta E_C^{\rm sp}$		2.406		2.117	1.893			
$\frac{1}{2}_1^- \otimes d$			0.004			0.255		0.698
$\Delta E_C^{\rm sp}$			2.747			2.633		2.490
$\frac{5}{2}_1^- \otimes s$			0.042			0.016		0.108
$\Delta E_C^{\rm sp}$			2.602			2.479		2.240
$\frac{5}{2}_1^- \otimes d$	0.062	0.032	0.022	0.068	0.047	0.022	0.099	0.076
$\Delta E_C^{\rm sp}$	2.954	2.919	2.887	2.869	2.842	2.833	2.830	2.745
$\frac{3}{2}_2^- \otimes s$		0.002			0.013			
$\Delta E_C^{\rm sp}$		2.713			2.568			
$\frac{3}{2}_2^- \otimes d$	0.004	0.003	0.005	0.014	0.099	0.004	0.022	0.048
$E_> \otimes d$	0.042	0.095	0.048	0.037	0.043	0.064	0.064	0.036
$\Delta E_C^{\rm sp}$	2.973	2.941	2.911	2.895	2.871	2.863	2.860	2.790
$\Delta E_C^{\rm th}$	2.309	1.942	2.543	2.209	2.046	2.408	2.519	2.505
ΔE_x	−0.017	−0.030	−0.020	−0.129	−0.129	−0.051	−0.031	−0.128
$E_x^{\rm th}(^{12}{\rm N})$	1.197	1.764	3.143	3.081	3.449	4.048	4.237	5.334
$E_x^{\rm expt}(^{12}{\rm N})$	1.191	1.8(3)	3.132			(4.14)	(4.14)	5.348
ΔE (keV)	6	−36	11					−14

[a]Theoretical excitation energy.

[b]Not calculated since the $1s_{1/2}$ neutron in ^{12}B is unbound.

C. Coulomb energy shifts

In many cases, such as the present one, the low-lying abnormal-parity states in p-shell nuclei have a very simple structure, expressed in terms of an sd-shell nucleon, mainly $1s_{1/2}$ or $0d_{5/2}$, coupled to a few low-lying parent states of the core. The single-particle Coulomb energies for these orbits depend on the orbit and its binding energy, which makes the experimental Coulomb energy shifts a sensitive test of the wave function; for example, it is evident from the comparison of analog state energies in Fig. 2 that there are substantial shifts in excitation energy across an isospin multiplet, especially for states with a large $1s_{1/2}$ parentage. Because the structure of ^{12}N is rather poorly known, we try to estimate the binding energy differences between states in ^{12}B and ^{12}N. To do this, we compute single-particle Coulomb energies $\Delta E_C^{\rm sp}$ for each weak-coupling component and weight them by the shell-model parentages.

To obtain $\Delta E_C^{\rm sp}$, the depth of a Woods-Saxon well is adjusted to reproduce the neutron separation energy for a given component in ^{12}B. The Coulomb potential of a uniformly charged sphere is then added to the Woods-Saxon well and the proton separation energy for ^{12}N is calculated. In the case of unbound states, the complex energy $E - i\Gamma/2$ at which the scattering function has a pole is found using the code GAMOW [42]; this energy defines the resonance energy and single-particle width. The geometry of the Woods-Saxon well sets the overall scale of the direct Coulomb energy. The exchange energy and other small corrections, including charge symmetry breaking, which must be included in a first-principles attempt to calculate Coulomb energy differences, are ignored and effectively subsumed into the direct Coulomb energy; nevertheless, the direct Coulomb energy exhibits the orbit and binding energy dependence of the Coulomb energies. The parameters of the Woods-Saxon well are $r_0 = 1.26$ fm, $a = 0.60$ fm, and $V_{\rm so} = 6$ MeV (12 MeV for the code GAMOW [42]). The Coulomb radius parameter r_c is chosen to give the radius of the potential of a uniformly charged sphere, $R = \sqrt{5/3}\langle r^2 \rangle_{\rm ch}^{1/2}$. For ^{12}C, the rms charge radius is 2.472(15) fm [43], which gives $r_c = 1.394$ fm. The masses in amu (electron masses subtracted from atomic masses) are

TABLE IV. Experimental decay widths Γ^{expt} compared with predicted neutron decay Γ^{th} widths for states in ^{12}B and proton decay widths for states in ^{12}N. Γ^{sp} is the calculated width of a single-particle resonance, for the well geometry of Sec. IV.C., at an energy E_N above threshold for the specified decay channel.

	J^π	E_x (MeV)	Decay	E_N (MeV)	Γ^{sp} (keV)	Γ^{th} (keV)	Γ^{expt} (keV)
^{12}B	3^-	3.389	$n_0(d)$	0.019	0.0034	0.0030	0.0031(6)
	4^-	4.518	$n_0(d)$	1.148	145	118	110(20)
	3^-	5.726	$n_0(d)$	2.356	748	25.4	
			$n_1(d)$	0.231	1.6	1.1	50(20)
^{12}N	2^-	1.191	$p_0(s)$	0.590	124	87	118(14)
	1^-	1.764	$p_0(s)$	1.163	1173	894	750(250)
	3^-	3.132	$p_0(d)$	2.531	250	220	220(25)
	1^-	3.449	$p_0(s)$	2.848	[a]		
			$p_1(s)$	0.848	403	311	260(30)
	2^-	4.048	$p_0(d)$	3.447	640	290	
			$p_0(s)$	3.447	[a]		836(25)
	4^-	4.237	$p_0(d)$	3.636	749	610	744(25)
	3^-	5.348	$p_0(d)$	4.747	1614	55	
			$p_1(d)$	2.747	323	225	180(23)

[a]Too unbound for a single-particle $1s_{1/2}$ proton resonance.

$M(^{11}\text{B})=11.0066$, $M(^{11}\text{C})=11.0081$, $m_n=1.0087$, and $m_p=1.0073$. The ^{11}B+n and ^{11}C+p thresholds are at 3.370 and 0.601 MeV, respectively.

A breakdown of the calculation to predict the excitation energies of the eight low-lying negative-parity states (including an unknown but expected 0^- state) in ^{12}N from those of ^{12}B is given in Table III. The dominant parentages are to the $3/2^-$ ground state and the 2.125-MeV $1/2^-$, 4.445-MeV $5/2^-$, and 5.020-MeV $3/2^-$ excited states of ^{11}B. The corresponding excited states of ^{11}C are at 2.000, 4.319, and 4.804 MeV and the downward shifts of 125, 126, and 216 keV, respectively, are taken into account in a correction ΔE_x to the averaged single-particle Coulomb energy shift. The remaining parentage, denoted by $E_> \otimes d$ in Table III, is in part necessary to ensure proper elimination of spurious center-of-mass states. Some of this parentage is accounted for by $0s$-hole strength, particularly for the low-spin states, and some by parentage to $T=3/2$ states. We include the $E_>$ strength along with that for the $3/2^-_2 \otimes d$ strength (for the more deeply bound states, the single-particle Coulomb energies are high and not so orbit dependent, and this increased Coulomb energy would be partially compensated for by a decrease in Coulomb energy of the p-shell core states). The 1^-_2 and 2^-_2 model states have some $1s$ parentage to the $A=11$ ground state so that we cannot compute a Coulomb energy by our single-particle method, although we can obtain an upper limit by using the calculated $1s$ Coulomb energy for the most loosely bound $1s$ state (e.g., for the 1^-_1 state).

For the four known negative-parity levels of ^{12}N, the predicted excitation energies are in very good agreement with experiment, bearing in mind that the energy of the broad 1^-_1 level is not very well defined. Agreement of a similar quality is obtained using the same procedure for a number of other p-shell nuclei, in particular for the positive-parity states below 10 MeV in the neighboring ^{13}C, ^{13}N pair, which increases our confidence in the predictive power of such calculations. The predicted energy shifts cover a substantial range and exhibit clearly both the expected orbit and binding energy dependence, the latter being most evident for the lowest 2^-, 1^- doublet, where the Coulomb energy for the less bound 1^- state is $\sim$350 keV lower than that for the 2^- level. The energy shift associated with different core excitation energies is important for three states and is necessary to get agreement with the experimental energy of the 3^-_2 level. The predicted excitation energies for the 2^-_2 and 4^-_1 levels bracket the energy of the unresolved peak at 4.14 MeV in the ^{12}C(^{3}He,t)^{12}N reaction [31], in which a centroid shift with angle was noted. This shift is also evident in Fig. 1, and we have fitted the peak with two states. Finally, we note that the small predicted Coulomb energy shift for the 1^-_2 level leads to a large shift in excitation energy from 4.3 MeV in ^{12}B to $\sim$3.5 MeV in ^{12}N. This shift puts the level near to degeneracy with a level, possibly the 2^+_2 level, seen at 3.53 MeV via the ^{10}B(^{3}He,n)^{12}N reaction [44].

TABLE V. Parentages for states in the giant-resonance region.

	1^-_3	1^-_4	1^-_5	2^-_3	2^-_4
$\frac{3}{2}^-_1 \otimes s$	0.056	0.004	0.006	0 005	0.021
$\frac{3}{2}^-_1 \otimes d$	0.579	0.289	0.158	0.446	0.275
$\frac{1}{2}^-_1 \otimes s$		0.057			
$\frac{1}{2}^-_1 \otimes d$	0.104	0.105	0.001	0.400	0.088
$\frac{5}{2}^-_1 \otimes s$				0.015	0.062
$\frac{5}{2}^-_1 \otimes d$	0.127	0.030	0.027	0.042	0.010
$\frac{3}{2}^-_2 \otimes s$	0.048	0.097	0.610	0.021	0.310
$\frac{3}{2}^-_2 \otimes d$	0.011	0.353	0.061	0.027	0.173
$E_>$	0.075	0.065	0.137	0.044	0.061
$E_x(^{12}\text{N})$	7.1	7.8	8.5	6.1	6.8

D. Nucleon decay widths

Nucleon decay widths for unbound negative-parity states in ^{12}B and ^{12}N can be estimated by taking the single-particle widths of resonances in a potential well [42], with the depth adjusted to produce a resonance at the decay energy for the neutron or proton, and multiplying these by the shell-model spectroscopic factors given in Table III. This method will not work for s-wave neutron decay of ^{12}B or when the decay energy is too high for a well-defined single-particle resonance to exist, as is the case (noted in Table IV) for the s-wave ground-state decays of the 1^-_2 and 2^-_2 levels of ^{12}N; for the $\sim$4.1-MeV 2^- state, in particular, s-wave p_0 decay is probably a major contributor to the width. Aside from these limitations, it can be seen from Table IV that there is generally good agreement between the calculated widths and the experimental values. Some small contributions to the widths, such as d-wave competition to dominant s-wave decay or small p_1 branches, have been omitted from Table IV.

It is also of interest to look at the structure and widths of the higher states that give rise to the dipole and spin-dipole strength centered around 7 MeV in ^{12}N. Parentage decom-

TABLE VI. Partial widths for states in the giant-resonance region. The symbols are defined in Table IV and all energies are in MeV. The widths are d wave unless otherwise specified. We estimate that the width for s-wave p_3 decay from the 2_4^- level is about 0.6 MeV and that the 1_5^- level should be rather broad on account of the same decay channel (see Table V).

	J^π	E_x	N_n	E_p^{expt}	Γ^{sp}	Γ^{th}	Γ^{tot}
^{12}B	2_3^-	6.52	n_0	3.15	1.45	0.65	
			n_1	1.03	0.10	0.04	0.69
	2_4^-	7.27	n_0	3.90	2.40	0.66	
			n_1	1.78	0.37	0.03	0.69
	1_3^-	7.56	n_0	4.19	2.85	1.65	
			n_1	2.07	0.55	0.06	1.71
	1_4^-	8.34	n_0	4.97	4.35	1.26	
			n_1	2.85	1.15	0.12	1.38
^{12}N	2_3^-	6.07	p_0	5.47	2.42	1.08	
			p_1	3.47	0.65	0.26	1.34
	2_4^-	6.76	p_0	6.16	3.37	0.93	
			p_1	4.16	1.13	0.10	1.03
	1_3^-	7.13	p_0	6.53	4.03	2.33	
			p_1	4.53	1.42	0.15	2.48
	1_4^-	7.84	p_0	7.24	5.50	1.59	
			p_1	5.24	2.16	0.23	1.82

positions for the 1_3^-, 1_4^-, 1_5^-, 2_3^-, and 2_4^- states are given in Table V. Much of the parentage consists of d-wave strength based on the lowest two states of the core. There is also appreciable parentage to the $5/2_1^-$ and $3/2_2^-$ states at 4.3 and 4.8 MeV, respectively, in ^{11}C. In the case of the 1_5^- and 2_4^- states, there is substantial s-wave parentage. For this reason, these states should be very broad.

Calculated d-wave partial widths for n_0 and n_1 decay in ^{12}B and p_0 and p_1 decay in ^{12}N are given in Table VI. The excitation energies used in ^{12}B are taken from the shell-model calculation (normalized [17] to the known energy of the 4_1^- level), while those in ^{12}N are obtained from a rough estimate using a constant single-particle Coulomb energy for unbound d orbits of 2.4 MeV. While there will also be some s-wave width, the d-wave widths of $1-2$ MeV are of the right magnitude to explain the distribution of dipole strength seen in this, and other, charge-exchange reactions.

E. Distorted-wave calculations

Angular distributions were calculated in the distorted-wave impulse approximation (DWIA) using the code DW81 [40]. These calculations use the 140-MeV t-matrix NN interaction as parametrized by Franey and Love [45]. The density-dependent G-matrix interaction of Nakayama and Love [46], at the same energy, has also been used. The optical-model parameters are interpolated from the work of Comfort and Karp [47].

The nuclear structure input is taken from the $0\hbar\omega$ and $1\hbar\omega$ shell-model calculations described in the previous subsections. Core-polarization corrections, which take into account the effect of configurations not included in the model space, are expected to be substantial and to lead to a multipole-dependent quenching of cross sections for the isovector transitions of interest. Such effects follow from general properties of the effective NN interaction, as demonstrated in schematic models, perturbative mixing calculations and large-basis shell-model calculations; for example, the inclusion of $p^2 \rightarrow (sd)^2$ excitations leads to substantial quenching in dipole and spin-dipole transitions. Often such effects are included empirically by scaling selected OBDME to fit electron scattering form factors (for analog states). This scaling is best done in an LS representation; longitudinal form factors for normal-parity excitations are related to $\Delta S=0$ OBDME, while transverse form factors are usually controlled by $\Delta S=1$ OBDME. Also, core-polarization corrections can change the shapes of form factors (transition densities), particularly at high-momentum transfers, and this effect is sometimes mocked-up by changing the radial scale of the single-particle wave functions. Details are discussed on a state-by-state basis in the next section. Remaining discrepancies in the resultant (p,n) cross sections are exhibited by normalizing the angular distribution obtained from the DWIA calculation to the experimental angular distribution in the region of momentum transfer corresponding to the ΔL transfer where the cross section is maximum (see Figs. 6 – 13 in Ref. [17] for the cross sections corresponding to pure ΔL, ΔS excitations).

The conventional OBDME that result from model calculations, plus scaling if necessary, are transformed (essentially a Talmi-Moshinsky transformation for unequal masses) so that the single-particle wave functions are expressed in terms of the relative coordinate between the nucleon and the $A=11$ core [17]. When harmonic-oscillator single-particle wave functions are used, the appropriate oscillator parameter is $b_{\text{rel}}=\sqrt{A/(A-1)}b_0$ where $b_0=\sqrt{\hbar/m_p\omega}$. A value $b_0=1.64$ fm is required to fit the rms charge radius of ^{12}C in a p-shell model. The more realistic Woods-Saxon wave functions are explicitly a function of the relative coordinate. Cross sections calculated with Woods-Saxon wave functions are generally smaller on account of the lack of overlap between the deeply bound p-shell neutron in the initial state and the loosely bound, or unbound, proton in the final state [17,48].

V. COMPARISON BETWEEN EXPERIMENT AND THEORY

A. The 1^+ ground state

The angular distribution for the transition to the strongly excited 1^+ ground state of ^{12}N is shown in Fig. 3. This transition is a good example of a so-called Gamow-Teller (GT) excitation ($\Delta L=0$, $\Delta S=1$) with the (p,n) reaction. Shown also are 120-MeV ^{12}C(p,p') cross sections to the analog state at 15.11 MeV in ^{12}C [49], multiplied by a factor of 2 to account for the different isospin couplings in the projectile subspace. The agreement between the (p,n) and (p,p') measurements is quite good, especially at forward angles, confirming the absolute normalization of these data.

The solid curve in Fig. 3 represents a DWIA calculation with the 140-MeV t matrix, a set of OBDME adjusted to fit the (e,e') form factor of the 15.11-MeV level of ^{12}C (third line of Table VI in Ref. [17]) and an oscillator parameter $b_{\text{rel}}=1.9$ fm from the same fit (the large value for b_{rel} is

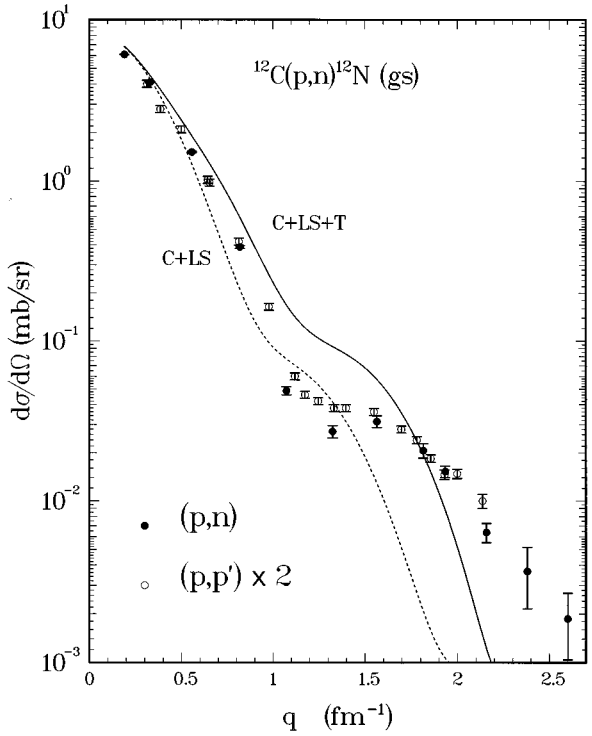

FIG. 3. Angular distribution (solid circles) for the ^{12}C$(p,n)^{12}$N reaction at 135 MeV to the 1^+ ground state. The open circles are 120-MeV (p,p') data ($\times 2$) for the transition to the analog state in ^{12}C [49]. The solid line represents a DWIA calculation using one-body density-matrix elements fitted to the (e,e') form factor of the analog level in ^{12}C (see text).

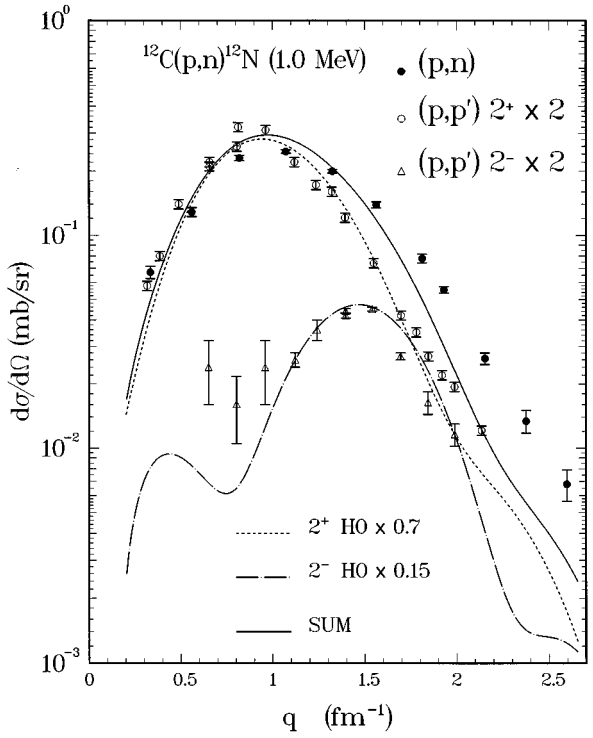

FIG. 4. Angular distribution (solid circles) for the ^{12}C$(p,n)^{12}$N reaction at 135 MeV to the 2^+, 2^- complex at 1.0 MeV. The open symbols are 120-MeV (p,p') data ($\times 2$) for the transitions to the analog states in ^{12}C, from Ref. [49]. The curves represent DWIA calculations using harmonic-oscillator wave functions with the normalizations shown. The transition densities, based on the p-shell calculation of Cohen and Kurath (CK) (Ref. [20]) for the 2^+ state and the $1\hbar\omega$ calculation of Millener and Kurath (MK) (Refs. [21,17]) for the 2^- state, have already been adjusted to fit electron scattering data in the case of the 2^+ state (see text).

simply an artifact of a fit using a restrictive p-shell model). At small angles, the DWIA calculation agrees quite well (to within 10%) with the experimental angular distribution. In the region of the shoulder around $q=1.3$ fm^{-1}, the DWIA calculation substantially overpredicts the cross section. The density-dependent G-matrix interaction of Nakayama and Love [46] gives a somewhat lower cross section in this region but the agreement with the data is still not good, in analogy to the findings of Bauhoff *et al.* [50] in an analysis of ^{12}C(p,p') data at 135 MeV. The problems are similar in the (p,n) reaction at 160 MeV [51] and in the (p,p') reaction at 200 MeV [52].

The $\Delta J=1$ cross sections involve a delicate interplay of $L=0$ and 2, or equivalently longitudinal and transverse, spin-dipole transition densities and interaction components [51]. In a p-shell model, the $L=0$ and $L=2$ densities can be adjusted to fit the (e,e') form factor [17] up to ~ 1.8 fm^{-1}. The $L=0$ density controls the low-q behavior or the GT strength (remembering that meson-exchange-current corrections are different for the two processes) and the $L=2$ density can be adjusted to reproduce the minimum of the form factor. The inclusion of higher configurations via core-polarization calculations [53] changes the $L=0$ and $L=2$ densities in such a way as to improve the agreement with the (e,e') data. At large momentum transfers, no p-shell model can reproduce the (e,e') form factor (transition density), and core-polarization calculations do little better, so that DWIA calculations using these transition densities cannot be expected to reproduce the (p,n) or (p,p') cross sections.

B. The 2^+, 2^- complex at 1.0 MeV

The first excited state of ^{12}N is known to be a 2^+ level at 0.96 MeV. Its analogs in ^{12}B and ^{12}C are at 0.95 MeV and 16.11 MeV, respectively. The 2^+ state in ^{12}N in this experiment is unresolved from a 2^- state at 1.19 MeV. The analogs of the 2^- state are at 1.67 MeV and 16.58 MeV in ^{12}B and ^{12}C, respectively. Figure 4 compares the ^{12}C(p,n) angular distribution for this doublet with the 120-MeV ^{12}C(p,p') angular distributions to the analog states [49], which could be resolved in that experiment. As for the ground state, the (p,p') cross sections were multiplied by a factor of 2 for comparisons here.

It is clear from Fig. 4 that the 2^+ state dominates the cross section for the 1 MeV peak. In a p-shell model, the two (of three) important OBDME for the 2^+ state, those with $\Delta L=2$ $\Delta S=0$ and $\Delta L=2$ $\Delta S=1$, can be scaled to give a good fit to the longitudinal and transverse (e,e') form factors, respectively, up to $q\sim 1.5$ fm^{-1}. For harmonic-oscillator wave functions, the scaling factors for the CKPOT interaction are 0.50 and 0.84 for the $\Delta S=0$ and $\Delta S=1$ OBDME [52]. The corresponding factors for Woods-Saxon wave functions are 0.577 and 0.915 (see Fig. 15 of Ref. [17]). Core-polarization calculations do reduce the transverse form factor near the peak and give a strong enhancement at large q [54], as required by the data. The curves in Fig. 4

from the DWIA calculations, which use the scaled OBDME and an oscillator parameter $b_{\rm rel}=1.71$ fm, determined by the rms charge radius, have been scaled down by a further factor of 0.7. This additional factor is typical of what has been found in analyses of (p,p') data [46,52]. Near the peak of the cross section, the central and tensor amplitudes are comparable and the strong constructive interference between these amplitudes leads to a slight overshoot of the data. For momentum transfers beyond the peak, the spin-orbit interaction also plays an important role (see Fig. 16 of Ref. [46]).

Clearly, little can be said from this experiment concerning the role of the 2^- state; nevertheless, this is a very interesting transition, for which the dominance of the $(\lambda\mu)=(2\ \ 1),\Delta L=1,\Delta S=1$ OBDME [17] gives rise to an (e,e') form factor peaked at high-momentum transfer. The (e,e') form factor is reproduced well with a normalization of 0.65 for harmonic-oscillator wave functions [32] (0.71 for the data of Deutschmann *et al.* [55]), while very little renormalization is required for Woods-Saxon wave functions; therefore, it is surprising that the DWIA calculations overestimate the measured cross section for this state by a factor of more than 5 [52]. Near the peak of the cross section, the tensor interaction dominates with some destructive interference from the central interaction. The magnitude of the peak cross section is quite insensitive to the choice of radial wave functions, although the position of the peak shifts with changes in radial scale. Because the structure of the state gives rise to a dominant $\Delta L=1$ amplitude, both longitudinal and transverse components of the effective interaction contribute. At higher energies (800 MeV), the (e,e') and (p,p') normalization factors are more nearly commensurate [56]. At low incident energies (35 and 40 MeV), the (p,n) cross section is much larger and peaks at low q ($\sim$0.7 fm^{-1}), where the cross section is very sensitive to the choice of radial wave function [48]; the cross section is reproduced well when the M3Y interaction is used with Woods-Saxon wave functions for the loosely-bound $\pi 1s_{1/2}$ and $\pi 0d_{5/2}$ orbits. It would be interesting to have low-q data at the higher bombarding energies. Further study of this and related transitions, such as the excitation of the $5/2_2^+$ state of ^{13}C or ^{13}N, would be of considerable interest.

C. The 1^- state at 1.8 MeV

The angular distribution for the broad 1^- state at 1.8 MeV is shown in Fig. 5. This transition is excited weakly and was observed only at three forward angles. Its analogs are at 2.62 MeV in ^{12}B and at 17.23 MeV in ^{12}C. The substantial shift in excitation across the multiplet, and the large width of the state in ^{12}C and ^{12}N, are consistent with the large $1s_{1/2}$ parentage to the $A=11$ ground state obtained in the shell-model calculations. Although the structure of the 1^- state is very similar to that of the 2^- member of the doublet at 1.19 MeV, there is a large enough $(\lambda\mu)=(1\ \ 0)$ amplitude [17] for the cross section to peak at low q rather than at high q. The shape of the calculated cross section fits the limited data quite well with a normalization factor of 0.20 if harmonic-oscillator wave functions are used. The peak of the cross section shifts to lower q when the more spatially extended Woods-Saxon wave functions are used and the cross section is reduced on account of the reduced

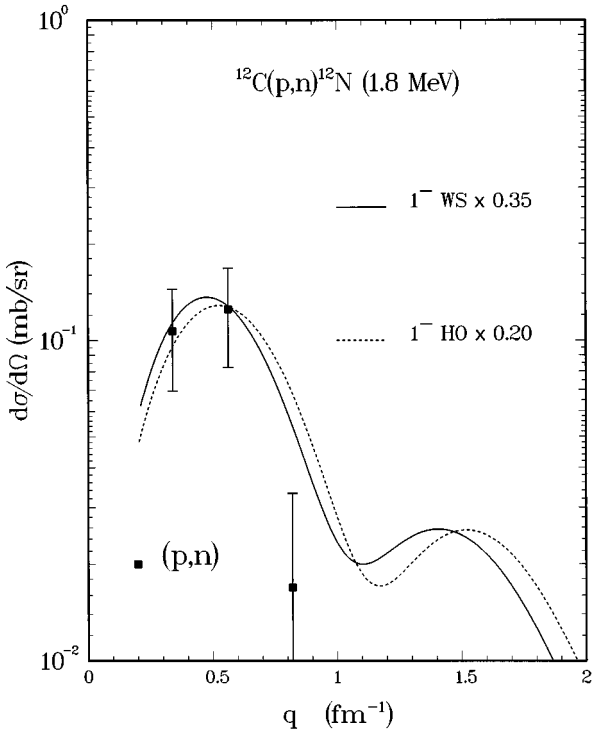

FIG. 5. Angular distribution for the ^{12}C$(p,n)^{12}$N reaction at 135 MeV to the 1^- state at 1.8 MeV. The solid and dashed curves represent DWIA calculations for the MK wave function using Woods-Saxon and harmonic-oscillator wave functions, respectively, with the normalizations shown.

overlap between initial- and final-state single-particle wave functions, with the normalization factor rising to 0.35. Previously, this state was observed only in the ^{12}C$(^3$He$,t)^{12}$N reaction [31], where the forward-peaked angular distribution is consistent with the $J^\pi=1^-$ assignment.

The (p,n) cross section at 135 MeV is largely a measure of the $(\lambda\mu)=(1\ \ 0)$, $\Delta S=1$ strength. The ground-state radiative width of the analog state at 17.23 MeV in ^{12}C is a measure of the $(1\ \ 0)$, $\Delta S=0$ strength and is given as $\Gamma_{\gamma_0}\geqslant 38.3$ eV [30]. This corresponds to $B(E1)\uparrow\geqslant 0.022\ e^2$ fm^2, which is consistent with the shell-model prediction of 0.038 e^2 fm^2.

D. Remaining states below 4.3 MeV

In a high-resolution study with the $(^3$He$,t)$ reaction [31], three relatively narrow peaks were observed at 2.45, 3.14, and 3.57 MeV. We do not see the 2.45-MeV 0^+ state, which has analogs in ^{12}B at 2.72 MeV and in ^{12}C at 17.76 MeV. There may be a small amount of strength near 2.4 MeV (see Fig. 1), but it is too small for us to extract a cross section. The predicted peak cross section for this state, without any renormalization, is less than 0.03 mb/sr at $q\sim 0.75$ fm^{-1}; the p-shell OBDME is necessarily pure $\Delta L=1$, $\Delta S=1$ and the cross section is due mainly to the tensor interaction. The other states appear as a complex seen as a shoulder on the larger complex of states centered near 4.3 MeV (see Fig. 1); for this reason, the extraction of cross sections for these states, which are excited weakly, is difficult and sensitive to the choice of line shapes and backgrounds. At forward

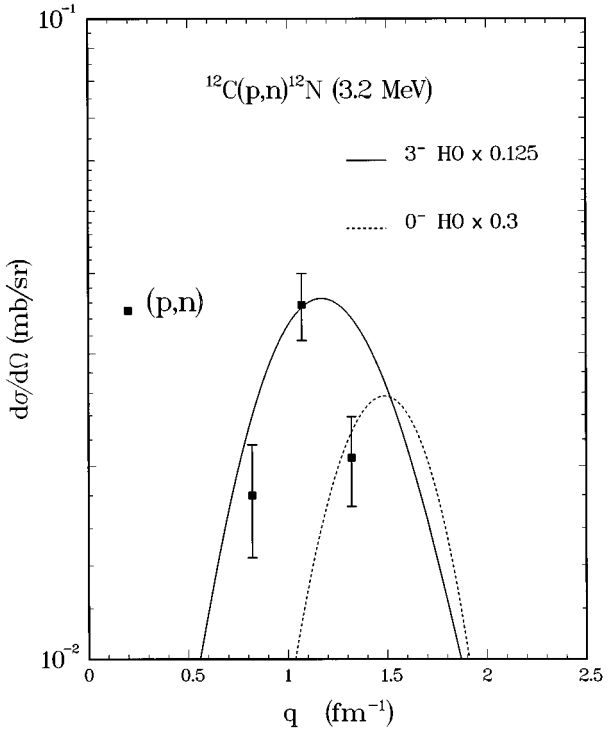

FIG. 6. Angular distribution for the $^{12}C(p,n)^{12}N$ reaction at 135 MeV to the 3^- state at 3.2 MeV. The solid curve represents a DWIA calculation for MK wave function using harmonic-oscillator wave functions with the normalization shown. The dashed curve shows a similar calculation for a 0^- state expected near this excitation energy.

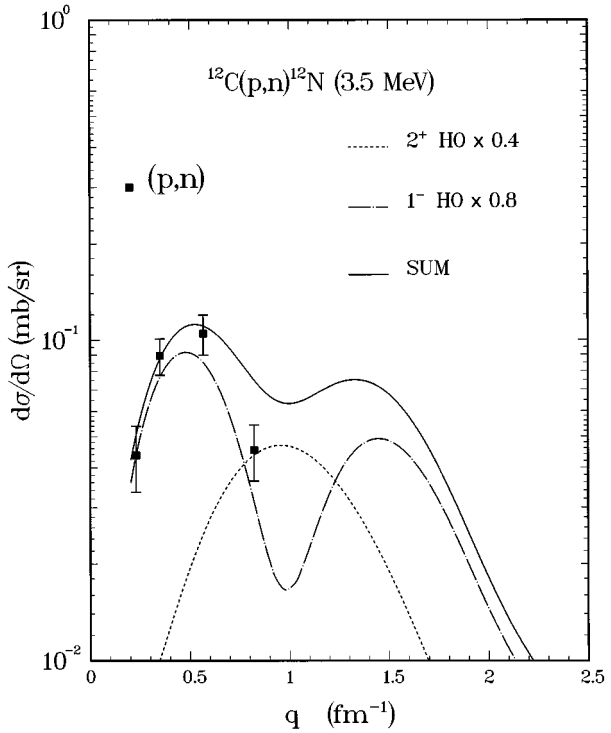

FIG. 7. Angular distribution for the $^{12}C(p,n)^{12}N$ reaction at 135 MeV to the 1^-, 2^+ complex at 3.5 MeV. The curves represent DWIA calculations for the MK and CK wave functions, respectively, using harmonic-oscillator wave functions with the normalization factors shown.

angles, we find evidence for cross section only at 3.5 MeV, and at wider angles only at 3.2 MeV.

The states expected in this region are the analogs of the 3.39-MeV 3^-, 3.76-MeV 2^+, and 4.30-MeV 1^- states of ^{12}B (18.35, 18.80, and 19.2 MeV in ^{12}C), along with the 0^- partner of the 1^- state (possibly at 18.40 MeV in ^{12}C). The 3^- and 1^- states in ^{12}N are expected, on the basis of our Coulomb energy calculations, to be near 3.1 and 3.5 MeV, respectively (see Table III).

The cross section that we extract for a state at $\sim$3.2 MeV is shown in Fig. 6 and is very small, reaching only $\sim$0.036 mb/sr at $q\sim1$ fm^{-1}. The three points do not seem to be consistent with any reasonable angular distribution. The DWIA calculation gives a cross section for the first 3^- state that is a factor of eight larger than what we extract, even after taking into account a quenching factor of two for spin excitations in the $0/1\hbar\omega$ model spaces. The calculated cross section at $q\sim1.2$ fm^{-1} receives comparable contributions from the central and tensor interactions, with constructive interference. The cross section for the predicted 0^- state is dominated by the tensor interaction, peaking at $q\sim1.5$ fm^{-1}, and is also larger than the extracted cross section (see Fig. 6). The (^{3}He,t) angular distribution is consistent with the excitation of a 3^- state, and the fairly large peak cross section of $\sim$0.2 mb/sr is probably due to the substantial non-spin-flip amplitude for the 3^-_1 model state, which is favored at the low incident energy per nucleon.

As can be seen from Fig. 7, the four low-q data points would be fitted well by the calculated cross section for the 1^- state without renormalization. The DWIA cross section for the second p-shell 2^+ state, which is expected also at about 3.5 MeV, is shown in Fig. 7 with a normalization factor of 0.4. This normalization, which takes into account the typical factor of two quenching for isovector spin excitations, gives a cross section comparable to that derived from Templon's analysis [57] of the region between strong peaks observed at 18.3 (mainly 2^-, $T=0$) and 19.4 MeV (mainly 2^-, $T=1$) in $^{12}C(p,p')$ at 156 MeV. From our data, it is hard to say anything definitive about the excitation of the 2^+ state. The peaking of the (^{3}He,t) cross section at small angles [31] is consistent also with the excitation of a 1^- state and the cross section at larger angles suggests a weak population of the 2^+ state (in Ref. [31], a tentative 1^+ assignment was discussed, but this seems unlikely given the lack of an analog in ^{12}B).

E. The 2^-, 4^- complex at 4.3 MeV

The angular distribution for the complex of states at 4.3 MeV is shown in Fig. 8. This complex is known to include a 2^- state and a 4^- state. Analogs of these states are observed at 4.46 MeV and 4.52 MeV in ^{12}B, and at 19.4 MeV and 19.65 MeV in ^{12}C, respectively (see Fig. 2). Figure 8 also shows DWIA calculations for transitions to the 2^-_2 state and the 4^-_1 state.

The overall shape of the complex is reproduced well with normalization factors of 0.4 and 0.5 for the transitions to the 2^- and 4^- states, respectively, if harmonic-oscillator wave functions are used (not shown) and 0.53 and 0.63 for Woods-

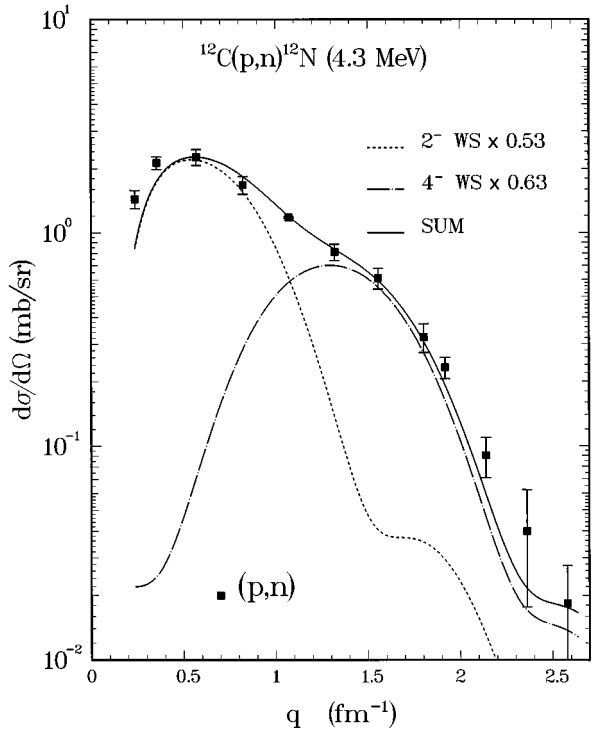

FIG. 8. Angular distribution for the ^{12}C$(p,n)^{12}$N reaction at 135 MeV to the 2^-, 4^- complex at 4.3 MeV. The curves represent DWIA calculations for the MK wave functions using Woods-Saxon wave functions with the *sd* orbits bound at 100 keV and with the normalizations shown.

Saxon wave functions (shown). Beyond $q\sim1.5$ fm^{-1}, the angular distribution is dominated clearly by the 4^- transition; hence, the normalization factor required for this state is not affected strongly by the details of the calculations for the lower-spin state in the complex; similarly, the 2^- state dominates at low q. This means that it is possible to obtain estimates of the excitation energies and widths of the 2^- and 4^- states from analyses of the low-q and high-q data, respectively. In fits using Lorentzian line shapes folded with a Gaussian resolution function, whose width is taken from the ground-state fit, the excitation energies and widths for the two states are $E_x=4.18(5)$ MeV, $\Gamma=836(25)$ keV, and $E_x=4.41(5)$ MeV, $\Gamma=744(25)$ keV (see Table I). The forward angle results are in generally good agreement with the (^{3}He,t) result of 4.14(10) MeV and 830(20) keV [31]. The peak cross section of 2.2 mb/sr is somewhat lower than $\sim$3 mb/sr from a (p,n) measurement at 160 MeV [58], 2.8 mb/sr from a (p,n) measurement at 186 MeV [19], and 2.8 mb/sr from an (n,p) measurement at 98 MeV [18]. Fits using Gaussian line shapes, which are not as good as those using Lorentzians, give cross sections lower by $\sim$30%, excitation energies lower by $\sim$100 keV and slightly different widths.

There have been few analyses of the analog 19.6-MeV complex in ^{12}C from (p,p') reactions at incident energies close to those of the present experiment. The results of Templon at 156 MeV [57], in which Lorentzian line shapes were used, are in good agreement with the present results under the assumption of good isospin for the 2^- state in ^{12}C. The cross sections of Comfort *et al.* at 200 MeV [52], obtained from an analysis using Gaussian line shapes, are somewhat lower. The comparison of (p,n) and (p,p') cross sections for the 4^- state is complicated by the fact that a pair of isospin-mixed 4^- levels exist within the 19.6-MeV complex. This is particularly evident from the comparison of $(\pi^+,\pi^{+\prime})$ and $(\pi^-,\pi^{-\prime})$ cross sections [59]. Likewise, two 4^- states at 19.29 and 19.65 MeV are included with a 2^- state at 19.4 MeV in analyses of 400-, 600-, and 700-MeV (p,p') data [56]. The 2^- state also appears to be isospin mixed with a predominantly $T=0$, 2^- state at 18.3 MeV.

The 2_2^- model state contains a large fraction of the shell-model spin-dipole strength. The corresponding physical states are strongly excited at low q in (e,e'), (p,p'), and charge-exchange reactions; however, a substantial quenching of the $1\hbar\omega$ shell-model transition density is required to give agreement with the experimentally measured cross sections, especially if harmonic-oscillator single-particle wave functions are used in constructing the radial transition density. As noted by Brady *et al.* [17], two physical effects lead to substantial quenching. First, the reduced overlap between the deeply bound initial-state wave functions and the loosely bound, or unbound, final-state wave functions reduces the reaction cross sections. We find a reduction of $\sim$25% when the unbound final-state wave functions are approximated by Woods-Saxon wave functions bound at 100 keV. Second, as expected on the basis of the schematic model, the inclusion of $p^2\rightarrow(sd)^2$ excitations in the shell-model bases leads to substantial quenching of isovector dipole and spin-dipole excitations; for example, the inclusion of all states up to $4\hbar\omega$ for ^{16}O leads to a factor of 2 quenching for the spin-dipole matrix element to the lowest 2^-, $T=1$ state [15]. No such comprehensive shell-model calculations have been reported for ^{12}C.

The 4^- state carries a large fraction ($\sim$94%) of the shell-model $M4$ strength. This strength should be quenched for the same reasons as given above, but the backwards-going amplitudes from $p^2\rightarrow(sd)^2$ admixtures in the ^{12}C ground state should be less destructive than they are for the dipole and spin-dipole excitations.

F. The 3^+ and 3^- states at 5.4 MeV

The angular distribution for the peak at 5.4 MeV is shown in Fig. 9. This peak should contain the analogs (see Fig. 2) of the 5.61-MeV 3_1^+ and 5.73-MeV 3_2^- states in ^{12}B. Candidates for the ^{12}C analogs exist at about 20.5 and 20.6 MeV, respectively. The 20.6-MeV complex is clearly observed in inelastic scattering reactions on ^{12}C, but may also contain $\Delta T=0$ excitations, which obviate a direct comparison between (p,p') and (p,n) cross sections. In fact, the strong stripping strength observed at 20.6 MeV in the ^{11}B(d,n) reaction [60] cannot be accounted for by either of the $T=1$ states (from Table III, the 3^- state has very little ground-state parentage), but can be accounted for by the fourth shell-model 3^-, $T=0$ state predicted at about this energy. On the other hand, the transverse (e,e') form factors [32] should be mainly due to $\Delta T=1$ excitations.

As can be seen from Fig. 9, the predicted DWIA cross sections are comparable for the 3_1^+ and 3_2^- model states. The summed cross sections give a reasonably good reproduction of the data after renormalization by a factor of 0.25 for each

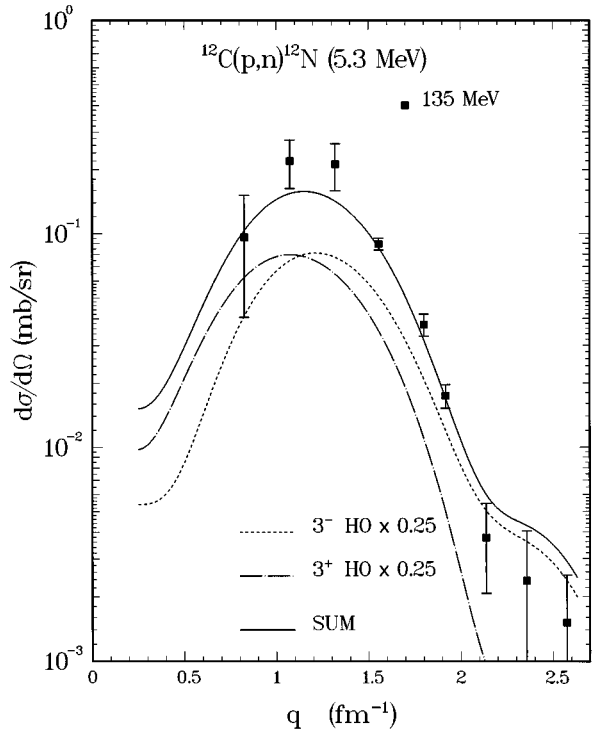

FIG. 9. Angular distribution for the ^{12}C$(p,n)^{12}$N reaction at 135 MeV to the 3^+, 3^- complex at 5.4 MeV. The curves represent DWIA calculations for CK and MK wave functions, respectively, using harmonic oscillator wave functions with the normalization factors shown.

state when harmonic-oscillator wave functions are used. [The summed transverse form factors, with the $E3$ form factor being about 2.5 times the $M3$ form factor, overestimate the (e,e') data by a similar factor [32].] The use of loosely bound (100 keV) Woods-Saxon wave functions results in (p,n) cross sections that are reduced by factors of 0.76 and 0.85 for the 3^+ and 3^- states, respectively. For the 3^+ state, the tensor interaction is dominant, while for the 3^- state, the central and tensor amplitudes are comparable with strong constructive interference.

It should be noted that the cross section extracted for the 5.4-MeV peak is sensitive to the assumed width (and background subtraction). The width of 180 keV adopted by Ajzenberg-Selove [30] is based mainly on the $(^3\mathrm{He},t)$ work of Sterrenberg *et al.* [31], who analyzed the peak as two states at 5.3 and 5.6 MeV with widths of 180(30) and 120(50) keV, respectively. Earlier $(^3\mathrm{He},t)$ work [61] gives a width of 400(80) keV for a single peak. This is consistent with the width (Table I) that we extract from the spectra at the two angles at which the peak is seen most clearly.

G. The dipole resonance region

The main peak of the giant dipole resonance in ^{12}C is centered at about 22.5 MeV [30]. In charge-exchange reactions, corresponding peaks, with widths of roughly $2-3$ MeV, are centered around 7.7 MeV in ^{12}B and slightly lower in ^{12}N. The $1\hbar\omega$ shell model predicts that this strength is due mainly to the excitation of 1^- states, with the $\Delta S=0$ and $\Delta S=1$ strength being nearly coincident in energy (e.g., Fig. 4 of Ref. [17]). Some 2^- strength is predicted at the low-energy side of the main 1^- strength, but the bulk of the 2^- spin-dipole strength is predicted in the 4.3-MeV peak. The ΔJ splitting of the spin-dipole strength, due to the spin-orbit interaction, puts the 0^- strength nearer to 10 MeV.

There is evidence from heavy-ion-induced charge-exchange reactions, which selectively populate spin-flip or non-spin-flip modes, that the dipole and spin-dipole strength in the $\sim$7-MeV peak is indeed essentially coincident in energy [62–66]. Also, in the (p,n) reaction, the strength of the 7-MeV peak relative to the 4-MeV peak (essentially pure $\Delta S=1$) gets progessively weaker as the incident energy increases [58], consistent with the energy dependence of the spin-independent part of the effective interaction.

Some structure is evident in the giant resonance region of ^{12}C; for example, the longitudinal $(\Delta S=0)$ strength observed at 22.0, 23.8, and 25.5 MeV via (e,e') [68] is consistent with the structure seen in photonuclear reactions [68,30]. There is less structure in the transverse response, although a peak is observed at 22.7 MeV [68,32]. The same peaks are seen in (p,p') reactions with $\Delta L=1$ angular distributions, except that the 23.8-MeV structure is resolved into two relatively narrow components at about 23.5 and 23.9 MeV [57,69]. In addition, the $(\vec{p},\vec{p}')$ reaction has been used to separate $\Delta S=0$ and $\Delta S=1$ contributions to the response [67]. We have chosen to analyze the strong dipole peak in our spectra in terms of peaks at 6.4 and 7.3 MeV, with widths of 1200 keV, on the basis of structure observed in the ^{12}C$(^3\mathrm{He},t)^{12}$N reaction [31,70]. We have also included peaks, with the same widths, at 8.2, 9.1, and 10.0 MeV to account for strength that is apparent in Fig. 2 above the fitted background on the high-energy side of the main dipole peak. Such a tail is observed in other experiments [18,19] and is expected on the basis of shell-model and RPA calculations [18,19]. The energies of the 8.2- and 10.0-MeV peaks coincide roughly with those of structure in the giant dipole resonance, referred to above, but the widths are chosen arbitrarily. Also, strength is observed at 9.9 MeV in the ^{12}C$(^3\mathrm{He},t)^{12}$N and ^{12}C$(^3\mathrm{He},tp)^{11}$C spectra of Ref. [70].

The angular distributions for all five states are shown in Fig. 10, together with the summed strength for the entire region. The angular distributions of the 6.4- and 7.3-MeV states, which are quite similar in shape and magnitude, are clearly consistent with the calculated dipole angular distributions of the third or fourth 1^- states, to which they are compared. The angular distributions for the 8.2- and 10.0-MeV states also appear to be dipole in nature, while the strength at 9.1 MeV is rather weak.

For reference, the predicted cross sections at $q=0.52$ fm^{-1} for pure dipole, spin-dipole 1^-, and spin-dipole 2^- states, using harmonic-oscillator wave functions, are 2.97, 12.07, and 13.38 mb/sr, respectively. The cross sections for the central interaction alone are 2.97, 6.43, and 11.63 mb/sr. For the tensor interaction alone, the cross sections are 0, 1.06, and 3.11 mb/sr. Thus, there is strong constructive interference between the central and tensor interactions for the 1^- spin-dipole state; the effect of the tensor force on the angular distribution can be seen by comparing the theoretical curves for the 1_3^- and 1_4^- model states in Fig. 10. The 1_4^- model state contains more than half of the dipole and spin-dipole strength predicted in this region [17]. The 1_3^- model

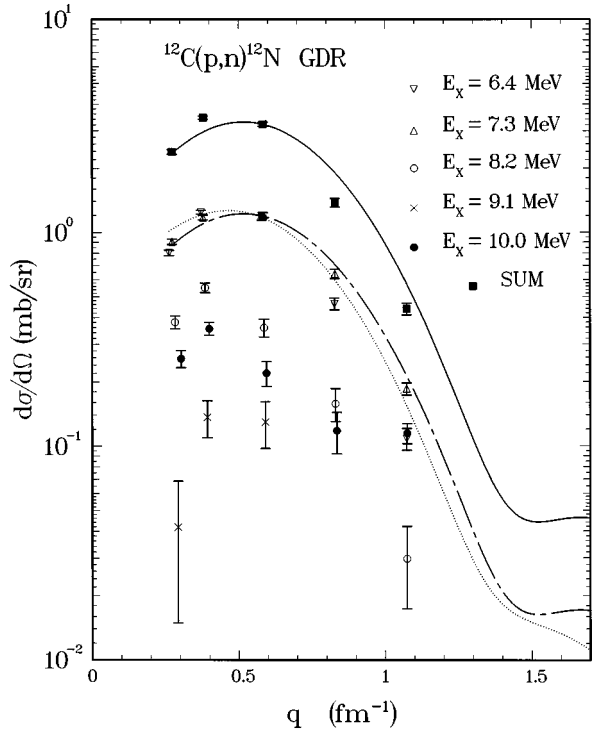

FIG. 10. Angular distribution for the ^{12}C$(p,n)^{12}$N reaction at 135 MeV to the assumed 1^- states at 6.4, 7.3, 8.2, 9.1, and 10.0 MeV. The solid and chain-dashed curves represent DWIA calculations for the 1_4^- MK state with normalizations of 0.89 and 0.33, respectively, using Woods-Saxon wave functions with *sd* orbit bound at 100 keV. The dotted curve represents a DWIA calculation for the 1_3^- MK state with a normalization of 1.05.

state carries most of the $\Delta S=0$ dipole strength and has a calculated cross section which is one third that of the 1_4^- state on account of the relative weakness of the spin-independent interaction at 135 MeV. The predicted cross section for the 2_3^- and 2_4^- states, mostly due to the 2_4^- state, is about half that of the 1_4^- state. The 1_5^- state also contains considerable spin-dipole strength [17], which should be rather broadly distributed because of a large *s*-wave proton decay width to the 4.8-MeV $3/2^-$ state of ^{11}C (see Table V).

The near equality in cross section for the 6.4- and 7.3-MeV peaks, seen also for the (^{3}He,t) cross sections, suggests that the peaks contain comparable amounts of dipole and spin-dipole strength in contradiction to the detailed predictions of the $1\hbar\omega$ shell model. Thus, it is more appropriate to compare the summed strength (both absolute and relative to the 2^- spin-dipole strength at 4.2 MeV) to model predictions and to that observed in other experiments. The latter comparison is of particular interest because the subtraction of background in the giant resonance region is a difficult and not clearly defined procedure. The comparison in Table VII shows that our summed cross section of $\sim$3.3 mb/sr is slightly lower than that extracted in other (p,n) and (n,p) experiments at 100$-$200 MeV incident energy. The theoretical prediction for the summed 1_3^-, 1_4^-, 2_3^-, and 2_4^- model states is 7.9 mb/sr if harmonic-oscillator wave functions are used. We expect that this value would be reduced by a factor approaching 2 if more realistic radial wave functions were used and if an extended shell-model calculation to take into account ground-state correlations were performed; more specifically, the RPA calculations reported in Ref. [19] give $\sim$2/3 the $\Delta L=1$ cross section of the $(0+1)\hbar\omega$ shell-model calculation and our estimate for the ratio of the cross sections for the 2_2^- state with Woods-Saxon and harmonic-oscillator wave functions is $\sim$0.75 (see Sec. V 5).

TABLE VII. Peak cross sections for the giant dipole region from (p,p') ($\times 2$) and charge exchange reactions at 100–200 MeV incident energy.

Reaction	Incident energy (MeV)	Cross section (mb/sr)	Reference
(p,n)	135	3.3	This work
(p,n)	120	4.7	[58]
(p,n)	160	4.0	[58]
(p,n)	200	3.5	[58]
(n,p)	98	5.7	[18]
(p,p')	156	3.7	[57]
(p,n)	186	3.6	[19]
(n,p)	190	3.6	[19]

VI. SUMMARY AND CONCLUSIONS

The ^{12}C$(p,n)^{12}$N reaction was studied at 135 MeV with energy resolutions of 350–425 keV. Angular distributions were extracted for all peaks observed up through the region of the giant dipole resonance at an excitation energy of around 7 MeV. In most cases, the peaks are thought to contain contributions from more than one state and, where possible, peak fitting was carried out. The J^π assignments for some of the states are already known; for the other cases, identifications were made by comparing the angular distributions with DWIA calculations and by comparing with the known analog states in ^{12}C and ^{12}B. In this connection, the Coulomb energy shifts and nucleon decay widths were estimated theoretically for negative-parity states using the known spectrum of ^{12}B as a starting point, along with the shell-model structure of the states.

In the first few MeV, we see the 1^+ ground state, an unresolved complex containing the 2^+ state at 0.96 MeV and a 2^- state at 1.19 MeV, and a weakly excited 1^- state at 1.8 MeV. The analogs of these states are all well known. The (p,n) angular distributions agree with the analog (p,p') angular distributions for the 1^+ ground state and the $2^+,2^-$ complex at 1 MeV. We do not see the reported 0^+ state at 2.44 MeV, but this is not surprising because the predicted cross section is very weak.

From peak fitting, we see evidence for weakly excited states at 3.2 and 3.5 MeV, which form a shoulder to the strongly excited 4.3-MeV peak. These states should correspond to states seen clearly at 3.14 and 3.57 MeV via the ^{12}C(^{3}He,t) reaction. The major contributors to the cross sections for these two peaks are most likely the 3^- and 1^- analogs of states in ^{12}B at 3.39 and 4.30 MeV. The analog of the 3.76-MeV 2^+ state of ^{12}B may contribute also to the 3.5-MeV peak (see Fig. 7). Between 4.1 and 4.3 MeV, we see the $2^-,4^-$ complex with known analogs in ^{12}C and ^{12}B. At forward angles, the 2^- state is strongest, and at backward angles, the 4^- state dominates. This fact allowed

us to obtain estimates of the excitation energies and widths of the 2^- and 4^- states from analyses of the low-q and high-q data. At 5.4 MeV, we see clearly a peak with an angular distribution that could be described by the excitation of either the 3^+ or the 3^- states known in the analog nuclei, or by a combination of both (the predicted cross sections are comparable). Between 6 and 8 MeV, we see a broad distribution of strength described well by a $\Delta L=1$ angular distribution. We have analyzed this strength in terms of three peaks, with the two strongest ones, at 6.4 and 7.3 MeV, based on a previous analysis of (^{3}He,t) data [31]. These states carry a significant fraction of the 1^- dipole and spin-dipole strength, although there could be some 2^- strength in this region as well. A major difficulty in the giant resonance region, as in all such studies, is an uncertainty in the background contribution.

All the states below 6-MeV excitation energy in ^{12}B, and thus ^{12}N, and the essential features of the dipole and spin-dipole strength in the giant resonance region can be accounted for by $0\hbar\omega$ shell-model calculations for the positive-parity states and by $1\hbar\omega$ calculations for the negative-parity states. For these restricted model spaces, there are substantial core-polarization corrections to the shell-model transition densities to be used in inelastic scattering calculations. A major effect for the isovector transitions of interest is a substantial quenching of transition strength at low momentum transfer for most multipoles. The loose binding of the final-state single-particle wave functions makes it important to use realistic single-particle wave functions, although it is difficult to do this precisely for unbound final states in ^{12}N; the lack of overlap between initial- and final-state wave functions generally leads to substantial reductions in cross section compared to those calculated with harmonic-oscillator wave functions. In the absence of satisfactory multi-$\hbar\omega$ shell-model calculations for $A=12$, scaling factors for certain LS OBDME are introduced. With a few exceptions, this procedure results in a consistent description of (e,e') form factors and (p,n) angular distributions up to $q\sim 1.5-2$ fm^{-1}; the quenching factors show a systematic behavior for p-shell nuclei and are in qualitative agreement with perturbative estimates. A notable exception occurs for the 2_1^- level, not resolved in our (p,n) data but observed in (p,p'), where the (p,n) or (p,p') cross section is driven by the tensor force. At higher q, the (e,e') and (p,n) cross sections often exceed the distorted-wave predictions, a phenomenon clearly evident but not well understood for the ground-state transition (the excitation of particles to higher orbits by the tensor force is known to provide a significant contribution).

The good energy resolution of the present experiment has enabled us to extract cross-section data for more states than previous (p,n) experiments. The new states include the broad 1^- state at 1.8 MeV, the 3^- state at 3.13 MeV, the second 1^- state at 3.5 (this peak should also contain a contribution from the second 2^+ state) and a 3^+, 3^- doublet near 5.4 MeV; in addition, new information on the excitation energies and widths of the 2^- and 4^- members of the 4.3-MeV doublet has been extracted from the data at momentum transfers where one or another of the states dominates the cross section. The calculated shifts in excitation energy from ^{12}B to ^{12}N for negative-parity states are in good agreement with the data for known states of ^{12}N, and lend strong support to the assignment of a 1^- state in the 3.5-MeV complex. Likewise, the calculated proton decay widths for the negative-parity states are in generally good agreement with the widths extracted from (^{3}He,t) data and the present (p,n) data. The result is a better understanding of the spectrum of ^{12}N.

ACKNOWLEDGMENTS

We wish to thank the staff at the Indiana University Cyclotron Facility for help in mounting and running this experiment. This work was supported in part by the National Science Foundation and by the U.S. Department of Energy under Contract No. DE-AC02-76CH00016.

[1] J. Rapaport and E. Sugarbaker, Annu. Rev. Nucl. Part. Sci. **44**, 109 (1994).

[2] W. G. Love, A. Klein, M. A. Franey, and K. Nakayama, Can. J. Phys. **65**, 536 (1987).

[3] B. D. Anderson, T. Chittrakarn, A. R. Baldwin, C. Lebo, R. Madey, R. J. McCarthy, J. W. Watson, B. A. Brown, and C. C. Foster, Phys. Rev. C **31**, 1147 (1985).

[4] B. D. Anderson, C. Lebo, A. R. Baldwin, T. Chrittrakarn, R. Madey, J. W. Watson, and C. C. Foster, Phys. Rev. C **41**, 1474 (1990).

[5] A. Fazely, B. D. Anderson, M. Ahmad, A. R. Baldwin, A. M. Kalenda, R. J. McCarthy, J. W. Watson, R. Madey, W. Bertozzi, T. N. Buti, J. M. Finn, M. A. Kovash, B. Pugh, and C. C. Foster, Phys. Rev. C **25**, 1760 (1982).

[6] T. Chittrakarn, B. D. Anderson, A. R. Baldwin, C. Lebo, R. Madey, J. W. Watson, and C. C. Foster, Phys. Rev. C **34**, 80 (1986).

[7] B. D. Anderson, N. Tamimi, A. R. Baldwin, M. Elaasar, R. Madey, D. M. Manley, M. Mostajabodda'vati, J. W. Watson, W. M. Zhang, and C. C. Foster, Phys. Rev. C **43**, 50 (1991).

[8] N. Tamimi, B. D. Anderson, A. R. Baldwin, T. Chittakarn, M. Elaasar, R. Madey, D. M. Manley, M. Mostajabodda'vati, J. W. Watson, W.-M. Zhang, J. A. Carr, and C. C. Foster, Phys. Rev. C **45**, 1005 (1992).

[9] L. A. C. Garcia, B. D. Anderson, D. M. Manley, A. R. Baldwin, R. E. Pourang, E. Steinfelds, J. W. Watson, R. A. Lindgren, B. L. Clausen, A. D. Bacher, and C. C. Foster, Phys. Rev. C **50**, 289 (1994).

[10] I. S. Towner, *A Shell Model Description of Light Nuclei* (Clarendon, Oxford, 1977), Chap. 4.

[11] P. Ring and P. Schuck, *The Nuclear Many-Body Problem* (Springer-Verlag, New York, 1980), Chap. 8.

[12] T. W. Donnelly and G. E. Walker, Ann. Phys. (N.Y.) **60**, 209 (1970).

[13] F. A. Gareev, M. Gmitro, S. N. Ershov, and J. Ceipak, Sov. J. Nucl. Phys. **42**, 11 (1985).

[14] W. C. Haxton and C. Johnson, Phys. Rev. Lett. **65**, 1325 (1990).
[15] E. K. Warburton, B. A. Brown, and D. J. Millener, Phys. Lett. B **293**, 7 (1992).
[16] D. J. Millener, A. C. Hayes, and D. Strottman, Phys. Rev. C **45**, 473 (1992).
[17] F. P. Brady, T. D. Ford, G. A. Needham, J. L. Romero, D. S. Sorenson, C. M. Castaneda, J. L. Drummond, E. L. Hjort, B. McEachern, N. S. P. King, and D. J. Millener, Phys. Rev. C **43**, 2284 (1991).
[18] N. Olsson, H. Condé, E. Ramström, T. Rönnqvist, R. Zorro, J. Blomgren, A. Håkansson, G. Tibell, O. Jonsson, L. Nilsson, P.-U. Renberg, A. Brockstedt, P. Ekström, M. Österlund, S. Y. van der Werf, D. J. Millener, G. Szeflinska, and Z. Szeflinski, Nucl. Phys. **A559**, 368 (1993).
[19] X. Yang, L. Wang, J. Rapaport, C. D. Goodman, C. Foster, Y. Wang, W. Unkelbach, E. Sugarbaker, D. Marchlenski, S. de Lucia, B. Luther, J. L. Ullmann, A. G. Ling, B. K. Park, D. S. Sorenson, L. Rybarcyk, T. N. Taddeucci, C. R. Howell, and W. Tornow, Phys. Rev. C **48**, 1158 (1993).
[20] S. Cohen and D. Kurath, Nucl. Phys. **73**, 1 (1965).
[21] D. J. Millener and D. Kurath, Nucl. Phys. **A255**, 315 (1975).
[22] A. R. Baldwin and R. Madey, Nucl. Instrum. Methods **171**, 149 (1980).
[23] R. Madey, J. W. Watson, M. Ahmad, B. D. Anderson, A. R. Baldwin, A. L. Casson, W. Casson, R. A. Cecil, A. Fazely, J. M. Knudson, C. Lebo, W. Pairsuwan, P. J. Pella, J. C. Varga, and T. R. Witten, Nucl. Instrum. Methods **214**, 401 (1983).
[24] P. R. Bevington, *Data Reduction and Error Analysis for the Physical Sciences* (McGraw-Hill, New York, 1969), p. 237.
[25] B. D. Anderson, A. R. Baldwin, A. M. Kalenda, R. Madey, J. W. Watson, C. C. Chang, H. D. Holmgren, R. W. Koontz, and J. R. Wu, Phys. Rev. Lett. **46**, 226 (1981).
[26] B. D. Anderson, T. Chittrakarn, A. R. Baldwin, C. Lebo, R. Madey, P. C. Tandy, J. W. Watson, B. A. Brown, and C. C. Foster, Phys. Rev. C **31**, 1161 (1985).
[27] R. Cecil, B. D. Anderson, and R. Madey, Nucl. Instrum. Methods **161**, 439 (1979).
[28] J. W. Watson, B. D. Anderson, A. R. Baldwin, C. Lebo, B. Flanders, W. Pairsuwan, R. Madey, and C. C. Foster, Nucl. Instrum. Methods **215**, 413 (1983).
[29] J. D'Auria, M. Dombsky, L. Moritz, T. Ruth, G. Sheffer, T. E. Ward, C. C. Foster, J. W. Watson, B. D. Anderson, and J. Rapaport, Phys. Rev. C **30**, 1999 (1984).
[30] F. Ajzenberg-Selove, Nucl. Phys. **A506**, 1 (1990).
[31] W. A. Sterrenburg, M. N. Harakeh, S. Y. van der Werf, and A. van der Woude, Nucl. Phys. **A405**, 109 (1983).
[32] R. S. Hicks, J. B. Flanz, R. A. Lindgren, G. A. Peterson, L. W. Fagg, and D. J. Millener, Phys. Rev. C **30**, 1 (1984).
[33] D. Ashery, M. S. Zisman, G. W. Goth, G. J. Wozniak, R. B. Weisenmiller, and J. Cerny, Phys. Rev. C **13**, 1345 (1976).
[34] G. Mairle and G. J. Wagner, Nucl. Phys. **A253**, 253 (1975).
[35] C. C. Maples, University of California, Report LBL-253, 1971.
[36] D. Kurath and D. J. Millener, Nucl. Phys. **A238**, 269 (1975).
[37] D. Kurath, in *Clustering Phenomena in Nuclei: II*, Proceedings of the Second International Conference, College Park, Maryland, edited by D. A. Goldberg, J. B. Marion, and S. J. Wallace (National Technical Information Service, Springfield, Va, 1975), pp. 439–449.
[38] E. K. Warburton and B. A. Brown, Phys. Rev. C **46**, 923 (1992).
[39] D. J. Millener, unpublished.
[40] Program DWBA70, R. Schaeffer and J. Raynal, unpublished; J. R. Comfort, extended version DW81, unpublished.
[41] R. E. Segel, S. S. Hanna, and R. G. Allas, Phys. Rev. **139**, B818 (1965).
[42] T. Vertse, K. F. Pal, and Z. Balogh, Comput. Phys. Commun. **27**, 309 (1982).
[43] H. de Vries, C. W. de Jager, and C. de Vries, At. Data Nucl. Data Tables **36**, 495 (1987).
[44] H. Fuchs, K. Grabisch, D. Hilscher, U. Jahnke, H. Kluge, T. Masterson, and H. Morgenstern, Nucl. Phys. **A234**, 61 (1974).
[45] M. A. Franey and W. G. Love, Phys. Rev. C **31**, 488 (1985).
[46] K. Nakayama and W. G. Love, Phys. Rev. C **38**, 51 (1988).
[47] J. R. Comfort and B. C. Karp, Phys. Rev. C **21**, 2162 (1980).
[48] H. Ohnuma, M. Kabasawa, K. Furukawa, T. Kawamura, Y. Takahashi, A. Satoh, T. Nakagawa, K. Maeda, K. Miura, T. Niizeki, and H. Orihara, Nucl. Phys. **A467**, 61 (1987).
[49] J. R. Comfort, G. L. Moake, C. C. Foster, P. Schwandt, C. D. Goodman, J. Rapaport, and W. G. Love, Phys. Rev. C **24**, 1834 (1981).
[50] W. Bauhoff, S. F. Collins, R. S. Henderson, G. G. Shute, B. M. Spicer, V. C. Officer, K. A. Amos, I. Morrison, D. W. Devins, D. L. Friesel, and W. P. Jones, Nucl. Phys. **A410**, 180 (1983).
[51] J. Rapaport, D. Wang, J. A. Carr, F. Petrovich, C. C. Foster, C. D. Goodman, C. Gaarde, J. Larsen, C. A. Goulding, T. N. Taddeucci, D. Horen, and E. Sugarbaker, Phys. Rev. C **36**, 500 (1987).
[52] J. R. Comfort, G. L. Moake, C. C. Foster, P. Schwandt, C. D. Goodman, J. Rapaport, and W. G. Love, Phys. Rev. C **26**, 1800 (1982).
[53] T. Suzuki, H. Hyuga, A. Arima, and K. Yazaki, Phys. Lett. **106B**, 319 (1981).
[54] T. Sato, K. Koshigiri, and H. Otsubo, Z. Phys. **320**, 507 (1985).
[55] U. Deutschmann, G. Lahm, R. Neuhausen, and J. C. Bergstrom, Nucl. Phys. **A411**, 337 (1983).
[56] K. W. Jones, C. Glashausser, R. de Swiniarski, F. T. Baker, T. A. Carey, J. R. Comfort, W. Cornelius, J. L. Escudié, M. Gazzaly, A. Green, M. Haji-Saeid, N. Hintz, G. Igo, J. B. McClelland, J. W. Moss, S. Nanda, and C. A. Whitten, Phys. Rev. C **50**, 1982 (1994).
[57] J. A. Templon, Ph.D. thesis, Indiana University, 1993.
[58] C. Gaarde, J. S. Larsen, H. Sagawa, N. Ohtsuka, J. Rapaport, T. N. Taddeucci, C. D. Goodman, C. C. Foster, C. A. Goulding, D. Horen, T. Masterson, and E. Sugarbaker, Nucl. Phys. **A422**, 189 (1984).
[59] C. L. Morris, J. Piffaretti, H. A. Thiessen, W. B. Cottingame, W. J. Braithwaite, R. J. Joseph, I. B. Moore, D. B. Holtkamp, C. J. Harvey, S. J. Greene, C. F. Moore, R. L. Boudrie, and R. J. Peterson, Phys. Lett. **86B**, 31 (1979).
[60] G. H. Neuschafer, M. N. Stephens, S. L. Tabor, and K. W. Kemper, Phys. Rev. C **28**, 1594 (1983).
[61] C. F. Maguire, D. L. Hendrie, D. K. Scott, J. Mahoney, and F. Ajzenberg-Selove, Phys. Rev. C **13**, 933 (1976).
[62] W. von Oertzen, Nucl. Phys. **A482**, 357c (1988).
[63] S. Nakayama, T. Yamagata, M. Tanaka, M. Inoue, K. Yuasa, T. Itahashi, H. Ogata, N. Koori, and K. Shima, Phys. Rev. Lett. **67**, 1082 (1991); Nucl. Phys. **A538**, 627c (1992).
[64] T. Ichihara *et al.*, Nucl. Phys. **A583**, 109c (1995); **A569**, 287c (1994); **A577**, 93c (1994); Phys. Lett. B **323**, 278 (1994).
[65] C. Bérat, M. Buénerd, J. Y. Hostachy, P. Martin, J. Barette, B.

Berthier, B. Fernandez, A. Miczaïka, A. Villari, H. G. Bohlen, S. Kubono, E. Stiliaris, and W. von Oertzen, Nucl. Phys. **A555**, 455 (1993).

[66] H. Okamura, S. Ishida, N. Sakamoto, H. Otsu, T. Uesaka, T. Wakasa, Y. Satoh, T. Fujita, H. Sakai, T. Niizeki, K. Katoh, T. Yamamoto, T. Yamashita, Y. Hara, H. Ohnuma, T. Ichihara, and K. Hatanaka, Nucl. Phys. **A577**, 89c (1994).

[67] F. T. Baker, D. Beatty, L. Bimbot, V. Cupps, C. Djalali, R. W. Fergerson, C. Glashausser, G. Graw, A. Green, K. Jones, M. Morlet, S. K. Nanada, A. Sethi, B. H. Storm, W. Unkelbach, and A. Willis, Phys. Rev. C **48**, 1106 (1993).

[68] A. Yamaguchi, T. Terasawa, K. Nakahara, and Y. Torizuka, Phys. Rev. C **3**, 1750 (1971).

[69] M. Buenerd, P. Martin, P. de Saintignon, and J. M. Loiseaux, Nucl. Phys. **A286**, 377 (1977).

[70] M. N. Harakeh, H. Akimune, I. Daito, Y. Fujita, M. Fujiwara, M. B. Greenfield, T. Inomata, J. Jänecke, K. Katori, S. Nakayama, H. Sakai, Y. Sakemi, M. Tanaka, and M. Yosoi, Nucl. Phys. **A577**, 57c (1994).